Hindawi
Advances in Polymer Technology
Volume 2020, Article ID 7310657, 14 pages
https://doi.org/10.1155/2020/7310657

Research Article

Polymethacrylate Sphere-Based Assay for Ultrasensitive miRNA Detection

Samira Hosseini,[1,2] **Patricia Vázquez-Villegas**,[1] **Richard C. Willson**,[3,4,5] **Marco Rito-Palomares**,[5] **Margarita Sanchez-Dominguez**,[6] **Leo H. Koole**,[6] **Marc J. Madou**,[7,8,9] **and Sergio O. Martínez-Chapa**[1]

[1]*Escuela de Ingenierı́a y Ciencias, Tecnologico de Monterrey, Ave. Eugenio Garza Sada 2501, Monterrey 64849, NL, Mexico*
[2]*Writing Lab, TecLabs, Vicerrectoría de Investigación y Transferencia de Tecnología, Tecnologico de Monterrey, Ave. Eugenio Garza Sada 2501, Monterrey 64849, NL, Mexico*
[3]*University of Houston, Department of Chemical and Biomolecular Engineering, Houston, TX 77204, USA*
[4]*University of Houston, Department of Biology and Biochemistry, Houston, TX 77204, USA*
[5]*Escuela de Medicina y Ciencias de Salud, Tecnologico de Monterrey, Avenida Ignacio Morones Prieto 3000 Poniente, 64710 Monterrey, NL, Mexico*
[6]*Centro de Investigación en Materiales Avanzados, S. C. (CIMAV), Unidad Monterrey, Parque de Investigación e Innovación Tecnológica, Apodaca, NL 66628, Mexico*
[7]*Faculty of Health, Medicine and Life Sciences, Maastricht University, Maastricht, Netherlands*
[8]*University of California, Department of Biomedical Engineering, Irvine, CA 92697, USA*
[9]*University of California, Department of Mechanical and Aerospace Engineering, Irvine, CA 92697, USA*

Correspondence should be addressed to Samira Hosseini; samira.hosseini@tec.mx

Received 3 July 2019; Revised 26 October 2019; Accepted 11 November 2019; Published 1 April 2020

Academic Editor: Leandro Gurgel

Although microRNAs (miRNAs) have emerged as increasingly important target analytes, their biorecognition remains challenging due to their small size, high sequence homology, and low abundance in clinical samples. Nanospheres and microspheres have also gained increasing attention in biosensor applications due to their high specific surface area and the wide variety of compositions available. In this study, chemically designed and synthesized microspheres with active functional groups were used to promote effective miRNA immobilization resulting in better biorecognition. Upon conjugation with fluorescence-labeled complimentary probes, acylate-based spheres have indirectly detected MiR159, offering significantly enhanced analytical sensitivity, specificity, and accuracy while yielding a considerably low limit of detection (LOD) of 40 picomolar. Furthermore, MiR159 presence, which is known to be inversely correlated to breast cancer incidence and progression, was successfully detected in a competitive assay, which is promising for upgrading the current assay to clinical use.

1. Introduction

MicroRNAs (miRNAs) are short regulatory ribonucleic acids (RNAs) ranging from 18 to 25 nucleotides in length [1]. Overexpression or underexpression of miRNAs is associated with various diseases and with distinct stages of specific illnesses [2–6]. Monitoring changes in expression levels of miRNAs is invaluable for timely initiation of treatment and/or for monitoring the effectiveness of an ongoing treatment [7–9]. MiRNAs are challenging targets for biorecognition due to their small size, high levels of sequence homology, and semistable secondary structures [10]. Routinely applied strategies for detection of miRNAs including northern blot, microarrays, or real-time polymerase chain reaction (PCR) require complex equipment and data analysis, while they are costly and not always available in every clinical setup [8, 11]. Moreover, several reports indicate insufficient specificity and sensitivity

when dealing with these techniques which add to the existing challenges of miRNA detection [12].

Nano/microspheres have drawn a great deal of interest in immunoassays due to their key advantageous features including (i) amenability to screening and multiplexing; (ii) significantly larger specific surface area in comparison with two-dimensional (2D) platforms which facilitate higher analyte-surface interaction; and (iii) high spatial freedom for interaction with biomolecules of interest [13–21]. miRNA detection using different particle types are reported in the literature [22, 23]. A wide range of particles were used for the purpose of miRNA detection including magnetic, carbon, graphene oxide, silver, and copper particles [24–30]. Quantum dots-encoded microbeads (Qbeads) introduce another strategy for detection of miRNAs [31, 32]. While these technologies opened windows of opportunity for effective detection of miRNAs, a vast majority of them involve time-consuming functionalization steps, expensive reagents, complicated procedures, and sophisticated laboratory setups [12]. Even then, the stability of the modified bioreceptive surfaces is not guaranteed, as they might lose their functionality over time [33, 34].

In this work, we describe a proof-of-concept strategy that involves cross-linked polymethacrylate microspheres of different sizes as bioreceptor surfaces for miRNA detection based on nucleotide hybridization. The polymer-based microspheres possess tailored physical and chemical properties. While offering a large surface area for analyte-surface interaction, the spheres are benefited from the inherent presence of carbonyl (-C=O), hydroxyl (-OH), and aromatic groups that further promotes biomolecular interactions. This makes the functionalization and surface activation steps unnecessary. Microspheres were integrated into a conventional 96-well plate for a one-step hybridization assay for biorecognition of Cy3-labeled miR159 as the target analyte, using a complementary amino-modified DNA capture probe. Moreover, synthetic unlabeled miR159 was detected in a competitive assay as a further proof-of-concept since the concentration of miR159 in blood serum is inversely correlated to the breast cancer incidence and progression in humans [35]. This straightforward strategy for the first time allows a routine analytical assay to detect microRNAs in the picomolar (pM) range without any amplification.

2. Materials and Methods

2.1. Chemicals and Reagents. Sodium citrate ($Na_3C_6H_5O_7$), sodium chloride (NaCl), hydrochloric acid (HCl), sodium dodecyl sulfate (SDS), polysorbate 20 (Tween 20), toluidine blue (TB), sodium hydroxide (NaOH), acetic acid (AcOH), nuclease-free water, and bovine serum albumin (BSA) were purchased from Sigma Aldrich (St. Louis, MO, USA). Capture probe, amino-modified DNA (5′-TTTAAGGAGCTCacatacgcgggcc-3′/amino modifier/), target Cy3-labeled analyte miR159 (5′-GAGCUCCUUAAAguuaaaca-3′/Cy3/), synthetic target miRNA159 (5′-GAGCUCCUUAAAguuaaaca-3′) and the noncomplementary negative control, Cy3-tagged miR-lin4 (5′-acaccugggcucuccggguac-3′/Cy3/), were purchased from Integrated DNA Technologies (Coralville, IA, USA). The uppercase and lowercase letters in the biomolecules represent complementary and noncomplementary nucleotides, respectively (amino modifier is a primary amine with no spacer arm).

2.2. Microsphere Synthesis. Polymethacrylate microspheres were synthesized in a suspension by polymerization (Geleen, the Netherlands) with monomers methyl methacrylate (MMA), 2 hydroxylethylmethacrylate (HEMA), 4-iodo-benzyloxo-ethyl methacrylate (4-IEMA), and tetraethyleneglycol dimethacrylate (TEGDMA). Details of particle synthesis and characterization (storage stability, hemo- and cyto-compatibility, structure, and absence of leachable components) have previously been reported [36, 37]. Spheres were sieved and size-sorted as follows: MMS-1 (200–400 μm); MMS-2 (400–600 μm); MMS-3 (600–700 μm); and MMS-4 (700–900 μm) (Figure 1). The spheres are slightly hydrophilic and relatively dense (~1.3 g/mL) which are advantageous features for biorecognition applications, as the conjugated particles will sink in aqueous media without clustering. This, in turn, maximizes the contact with the analyte of interest.

2.3. Morphology, Size Distribution, Surface Area, and Raman Spectroscopy Analyses. A scanning electron microscope equipped with a field emission gun (FESEM, JEOL, JSM7600F, USA) was used for the morphological analysis of platinum-coated spheres from different size categories. The acceleration voltage of the instrument was 0.5 kV. The size distribution of each size category was calculated from optical microscope images of 500 ± 5 randomly selected spheres from each group (OLYMPUS, BX51TRF, Japan). The specific surface area of each size category (per 10 mg) was calculated from the size distribution analysis (Figure 1) [36]. Raman spectra were recorded on a Raman Spectrometer, LabRAM HR Evolution (Horiba, Japan), coupled to an Olympus BX-4 microscope. The wavelength used to excite the sample was 532 nm, which was provided with a Nd:YAG laser as an irradiation source. The specific conditions were as follows: laser ND filter 25%, accumulation time of 3 s, 6 accumulations, 600 lines/mm grating (500 nm), a hole of 50 micrometers.

2.4. Topography Analysis of Microspheres before and after miRNA Immobilization. The surface of the microspheres before and after miRNA immobilization was analyzed by atomic force microscopy (AFM, Asylum Research MFP3D SA) in the tapping mode in air. An Asylum Research model AC240TS-R3 rectangular tip was used to analyze the surface. The scans covered areas of 60×60 μm and 1×1 μm with a speed interval from 0.20 to 0.50 Hz. The frequency of the first nominal resonance was 70 kHz, the nominal spring constant was 2 N/m, and the nominal curvature radius was 9 ± 2 nm. Prior to AFM analysis, samples of microspheres were incubated in hybridization solution (1 μM of capture probe and 1 μM of the Cy3-miRNA analyte) for 2 hours followed by washing two times with SSC and 0.01X SSC, respectively.

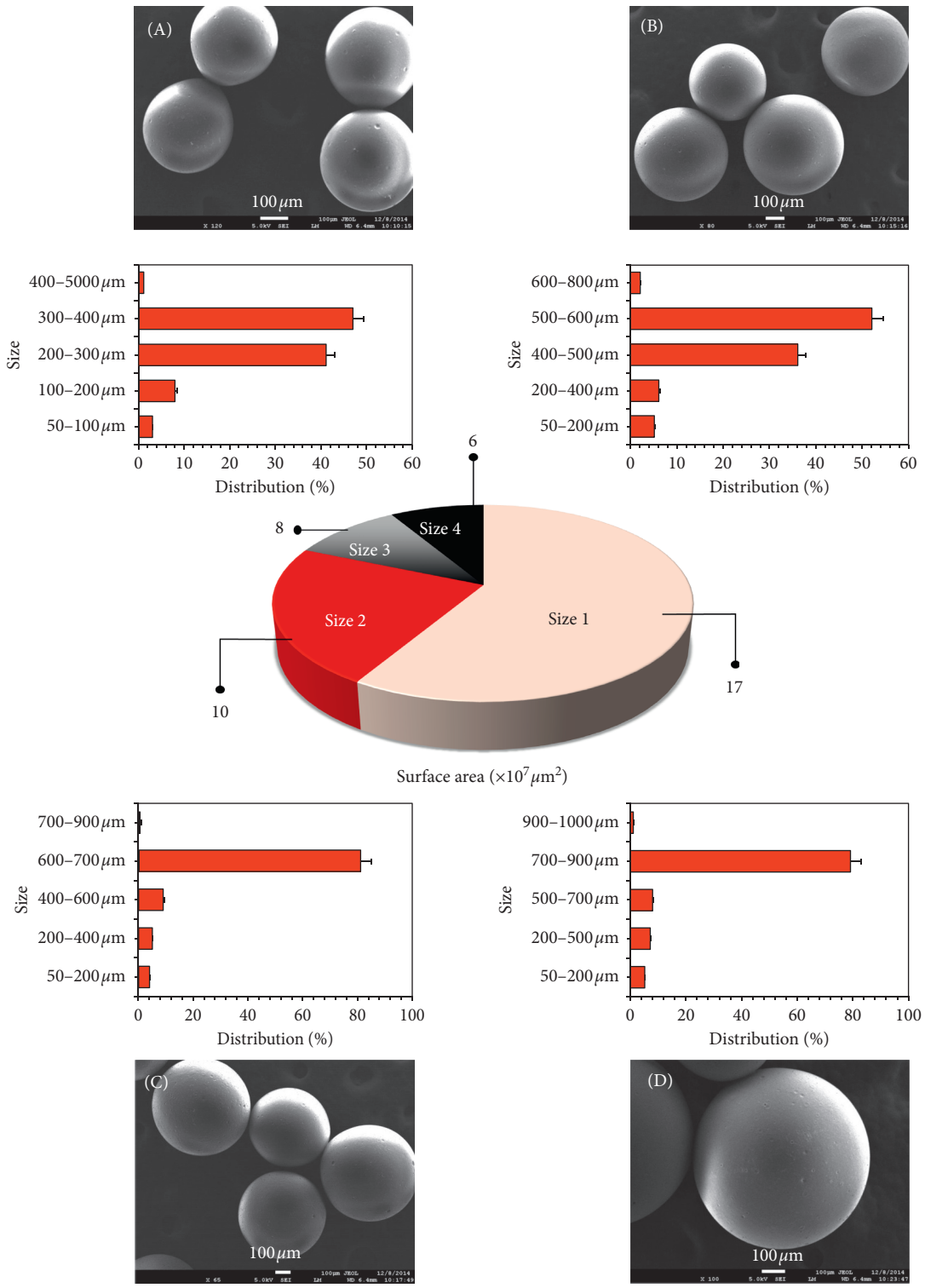

Figure 1: SEM images of the spheres from different size categories along with their size distributions: (a) MMS-1 (200–400 μm); (b) MMS-2 (400–600 μm); (c) MMS-3 (600–700 μm); (d) MMS-4 (700–900 μm). Specific surface area measurement for 10 mg of each size group is presented in the center.

2.5. Oligonucleotide Immobilization and Toluidine Blue Titration. The ability of the microspheres in accommodating miRNAs on their surface was assessed via a toluidine blue assay. The assay was calibrated prior to readout using calibration solutions of 2 μM, 4 μM, 6 μM, 8 μM, and 10 μM TB. Microspheres (10 mg) were incubated in a 1 μM solution of the capture probe (200 μL, 37°C, 2 h) followed by thorough washing with sodium saline citrate (SSC). This method was previously reported in the literature and was thoroughly tested [38–40]. Toluidine blue (TB) titration was used to

confirm the presence of the oligonucleotide capture probes bonded to the surface of the microspheres. This technique relies on the pH-dependent electrostatic interaction between TB dyes and nucleotide phosphate groups (Figure 2(a)) [38]. Spheres of different size categories (10 mg) were immersed in 8 mL of 0.5 mM TB and 0.1 mM NaOH solution for 2 hr, followed by washing the spheres in 0.1 mM NaOH for the complete removal of noncomplexed TB dye. The spheres were subsequently incubated in 3 mL of acidic solution (50% AcOH in distilled water) for 45 minutes in order to strip the complexed TB molecules into the acid solution for measurement at 635 nm by using a Jenway (Stone, Staffordshire, UK) spectrophotometer.

2.6. Buffer Preparation for the Analytical Assay. The stock solution of 20 times concentrated SSC (20X, 3 M NaCl, 0.3 M $Na_3C_6H_5O_7$, pH adjusted to 7 using HCl) and subsequent dilutions of this buffer (5X and 0.01X) were prepared with nuclease-free water (Sigma Aldrich, St. Louis, MO, USA). All dilutions were filtered with sterile 0.2 μm syringe filters (Corning, Corning, NY, USA). The capture probe solution was initially prepared in nuclease-free water and was diluted in SSC buffer to 10 μM. This concentration was utilized as the stock solution for further dilutions of the capture probe. The solutions of SSC and 0.01X SSC have been used as the washing buffers after incubation with the capture probe and hybridization miRNA, respectively. A blocking buffer containing (1%, w/v) BSA, (0.02%, w/v) SDS, and (0.05%, w/v) Tween 20 in 5X SSC was used to reduce the chance of nonspecific binding.

2.7. Indirect and Competitive Hybridization Assays. A predetermined amount of the spheres (10 mg) was loaded into the wells of conventional 96-well plates (Corning, NY, USA). As control, the indirect assay was also conducted in the conventional 96-well plate without spheres. To minimize experimental variability, all the assays were performed under the exact same conditions and by using the same batch of buffers. The miRNA probes were physically immobilized on the surface of the spheres. The spheres were loaded inside a 96-well plate, and each well was charged with 200 μL solution of capture probe (1 μM). The incubation was carried out for 2 hr at 37°C. All the wells were thoroughly washed with SSC buffer (3 times, 200 μL) and were charged with blocking buffer (200 μL) to avoid nonspecific binding. The incubation was carried out for 1 hr at 37°C followed by a complete washing process with SSC buffer. Each well has subsequently received 200 μL of the analyte solution (2 hr at 37°C). Analyte solutions (Cy3-miR159) were prepared by diluting the original concentration (100 μM) with 0.01X SSC buffer in order to achieve a concentration range as follows: 1000 nM, 100 nM, 10 nM, 1 nM, 100 pM, 10 pM, and 1 pM. To avoid fluorescent bleaching, from this step onwards, the assay was performed in a dark room. The assay was finalized by another round of washing (0.01X SSC) before readout. The fluorescence intensity of the Cy3 label was measured with 530/25 nm and 590/35 nm excitation and emission filters, respectively. The readout was performed with an integration time of 0.1 s and 120% sensitivity in a Synergy 2 microplate reader (BioTek Instruments, Inc., Winooskin, VT, USA).

Since the concentration of the target analyte is inversely correlated with breast cancer, a competitive hybridization assay was additionally performed to assess the potentials of the developed assay. Synthetic miR159 was detected in competition with Cy3-labeled miR159. In this procedure, 10 mg of microspheres (MMS- 3 as the representative group) was loaded in each well of a 96-well plate and coated with capture probe at 1 μM. The fluorescence-labeled miRNA (Cy3-miR159) was diluted to 100 nM and 1000 nM, while synthetic miR159 was diluted to 0 nM, 10 nM, 100 nM, and 1000 nM. Competitive binding was performed using the same buffers and at the same incubation time and temperatures as reported above. Relative fluorescent intensity was calculated by dividing intensity (for each concentration of the untagged miRNA) by the negative outcomes (calculated in the absence of untagged miRNA).

2.8. Calibration and Evaluation of the Assay. Calibration of the assay was performed with capture probe (1 μM) and different concentrations of the target analyte (1000 nM, 100 nM, 10 nM, 1 nM, 100 pM, 10 pM, and 1 pM). Calibration curves were plotted by conversion of the data to the logarithmic scale. Negative replicates were conducted with the noncomplementary Cy3-labeled miR-lin4 as hybridizing miRNA ($n = 10$). Cutoff values for each individual size category of the microspheres were calculated as twice that of the mean values of the negative controls [41]. Only readouts with intensity outcomes above cutoff values were interpreted as positives.

A total number of 80 positive and 40 negative replicates were conducted to obtain important parameters such as analytical sensitivity, specificity, and accuracy of the assay. Calculations were performed following the equations below considering the negative/positive readouts in comparison with the total number of the conducted replicates [42]:

$$\begin{aligned} \text{sensitivity} &= \frac{\text{TP}}{\text{TP} + \text{FN}} \times 100, \\ \text{specificity} &= \frac{\text{TN}}{\text{TN} + \text{FP}} \times 100, \\ \text{accuracy} &= \frac{\text{TP} + \text{TN}}{\text{total replicates}} \times 100. \end{aligned} \tag{1}$$

Variables in these equations are as follows:

True positive (TP)

True negative (TN)

False positive (FP)

False negative (FN)

Limit of detection (LOD) for each size category was determined as 3 times the average standard deviation (s, in the case of lowest miRNA concentration) divided by the slope of the calibration curve (m) following the given equation [34, 43–48]:

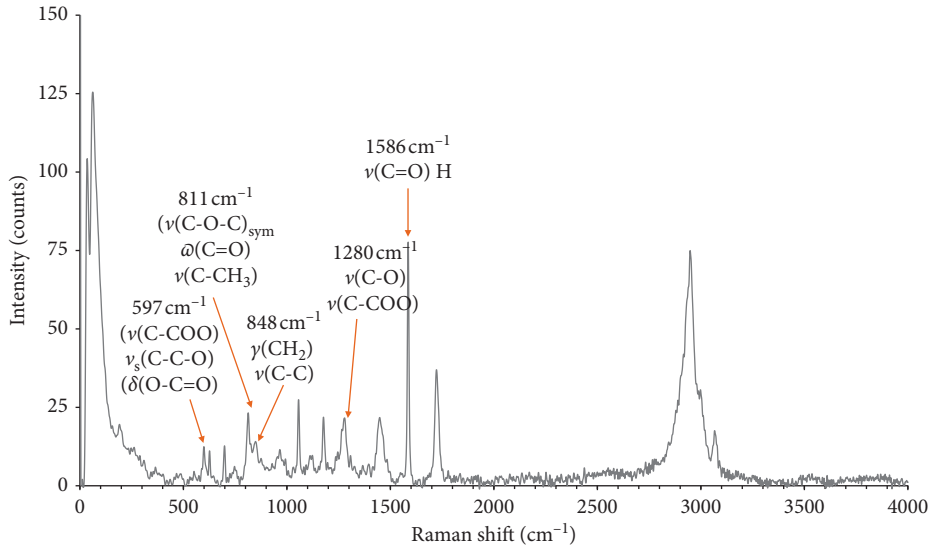

Figure 2: Raman analysis of the polymethacrylate spheres with the assigned peaks.

$$\text{LoD} = \frac{3 \times s}{m}. \quad (2)$$

The conventional assay conducted without spheres was also calibrated and carefully evaluated.

3. Results and Discussion

3.1. Morphology, Size Distribution, and Surface Area of the Spheres. Microspheres of different size groups were imaged by SEM, and representative morphologies are presented in Figures 1(a)–1(d). The recorded morphologies were found to be smooth, and the dimensions of the spheres were within the expected range as the sieved groups. Uniform spheres with consistent surface morphologies allow the interpretation to be focused on the effects of specific surface area and chemistry of the spheres for biomolecule immobilization.

Diameter range and size distribution (graphs in Figures 1(a)–1(d)) were calculated for each size group of the spheres by using optical images. Subsequently, the specific surface area for each size category was carefully calculated (for 10 mg of the microsphere) from the respective size distributions. The surface area ranged from 6×10^7 to 17×10^7 μm^2 (Figure 1, the central pie chart). As expected, the highest surface area per mass was offered by the smallest spheres (MMS-1), and the lowest specific surface area per mass was measured for the largest spheres (MMS-4). In principle, the higher specific surface area enhances the analyte-surface interaction resulting in higher probability of the biomolecular coupling and subsequent biorecognition [33, 49].

3.2. Raman Spectroscopy Analyses of the Spheres. Figure 2 shows the Raman spectrum of the microspheres. It should be noted that there is no signal from the C=C stretching mode from the methacrylic group, normally around 1640 cm^{-1}, indicative of successful copolymerization (an evidence for no free monomers) [50, 51]. Several signals were assigned to functional groups of the different polymers involved in synthesis of the spheres. The signal at 597 cm^{-1} may correspond to PMMA polymer (ν(C-COO), ν_S(C-C-O)) [52] as well as to p-HEMA (δ(O-C=O)) [53]. The peak at 811.8 cm^{-1} can be assigned to several signals from p-HEMA (ν(C-O-C)$_{sym}$, ϖ(C=O) or ν(C-CH$_3$)) [4]. Also arising from p-HEMA, the signal at 848 cm^{-1} can be assigned to γ(CH$_2$) or ν(C-C) [53]. The deformation localized on the OCH$_2$-CH$_2$OH part of the p-HEMA molecule can be seen at 955 cm^{-1} [53]. The signal at 1280.5 cm^{-1} can be assigned to ν(C-O) and ν(C-COO) from PMMA. At 1448.8 cm^{-1} [52], deformation from (C-CH$_2$) of p-HEMA can be observed [53]. The aromatic ring stretch from p-IEMA is shown at 1586.41 cm^{-1} [54]. Another signal from the carbonyl is observed at 1719.8 cm^{-1} (ν(C=O) H bonded from p-HEMA or p-TEGDMA) [55]. The wide band around 2949 cm^{-1} arises from several signals from PMMA (ν_S(C-H) of O-CH$_3$ with ν_S(C-H) of α-CH$_3$ and ν_a(CH$_2$)) [52]. Finally, the shoulder at 3065 cm^{-1} may arise from the iodobenzyl part of p-IEMA or various signals from PMMA and p-TEGDMA [52, 55].

3.3. Toluidine Blue (TB) Titration. The presence of negatively charged nucleotide strands on the surface of the spheres was investigated by a TB assay. As described before, each TB molecule contains an aromatic cation segment and a chloride anion (Figure 3(a)). A pH-sensitive adsorption/desorption mechanism leads to the ionization of the TB dye in the alkaline environment (Figure 3(a), step 1). Positively charged TB then binds to the negative $-PO_4^-$ groups of the miRNAs (Figure 3(a), step 2) and desorbs upon subsequent lowering of the pH (Figure 3(a), step 3). Concentration of the TB dyes measured by UV-Vis is expected to be proportional to the concentration of the capture probes on the surface of the microspheres.

Figure 3(b) shows a highly linear calibration plot for TB assay with predetermined concentrations of TB in acidic

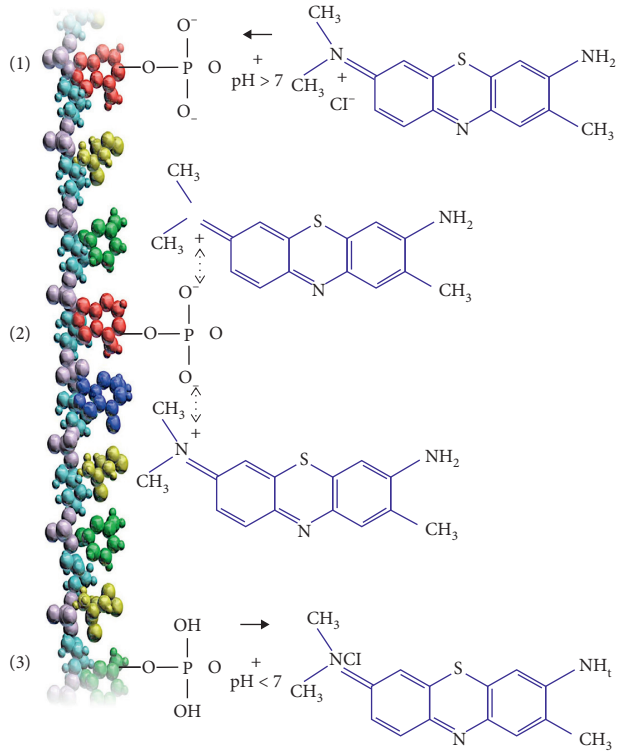

(a)

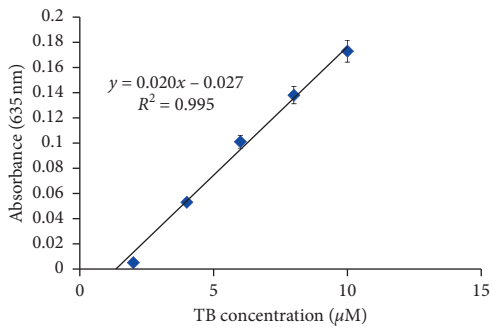

(b)

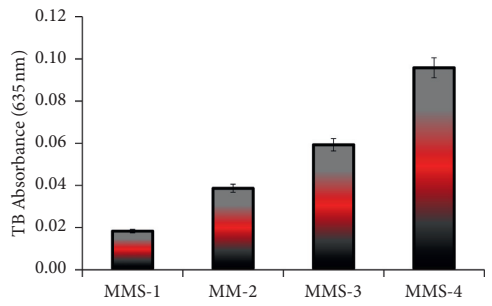

(c)

MMS groups	Surface area per 10 μg (mm^2)	TB bound (mM/mm^2)	Capture probe concentration (nM/mm^2)	Capture probe concentration (in 10 μg of the spheres) (nM)
1	170	95.0	3.80	645.8
2	100	171.1	6.84	684.4
3	80	226.1	9.04	723.5
4	60	330.3	13.21	792.7

(d)

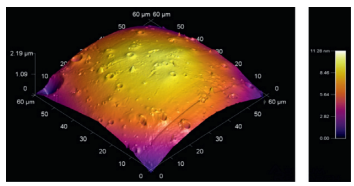

(e)

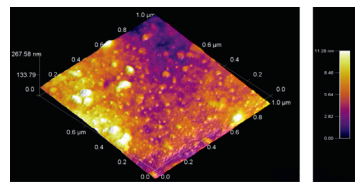

(f)

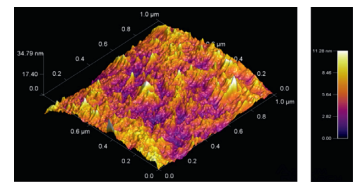

(g)

FIGURE 3: TB analysis for indirect confirmation of the presence of capture probe on the surface of the spheres: (a) adsorption and desorption mechanisms of the TB molecules to the $-PO_4^-$ groups of the nucleotide available on the surface of the spheres via alteration of the pH from the alkaline to acidic environment; (b) calibration curve plotted by titration of the TB assay using different concentrations of the calibration solutions (2 μM, 4 μM, 6 μM, 8 μM, and 10 μM); (c) TB absorbance per mm^2 of the surface measured by spectroscopic UV-Vis (635 nm); and (d) breakdown calculations of the TB assay. AFM analysis ((e) 60 μm) and zoomed-in view ((f) 10 μm) of the microspheres prior to immobilization and ((g) 10 μm) after surface attachment of the hybrid strands which shows the clear alteration of the surface roughness.

solution. While the concentration of TB is considered proportional to the concentration of the capture probe on the surface of the spheres, it is important to note that the results of TB assay is a comparative means for such correlation. Figure 3(c) represents the TB absorbance on 10 mg of the spheres from different size groups. As can be observed, the TB absorbance increases as the size of the spheres increases, which demonstrates that a higher particle size encourages a higher number of TB dye molecules to bind to the captured strands on the surface even though a lower total surface area is offered by the larger sizes. The latter is explained by the fact that spatial freedom for an efficient interaction between capture probes and TB molecules increases as the dimension of the spheres increases [49, 56, 57]. The approximate size of the TB molecules (≈0.7 to 1.1 nm) is in the range of the length of a horizontally oriented single miRNA strand (≈1 nm) on the beads so the more the space for maneuvering between the strands, the easier it is for TB to bind [58, 59]. Presumably available surface functionalities reacted with miRNA strands; thus, the inter-miRNA distance on the smaller particle size microspheres would make the TB diffusion rather difficult which is not the case when the larger sphere size is applied. In Figure 3(d), a breakdown calculation of the TB assay is provided. This analysis provides an approximate concentration of TB dyes per mm^2 of the spheres' surface. Every strand of the capture probe consists of 25 nucleotides with individual $-PO_4^-$ groups. It is known that TB is highly interactive towards anionic sulfates, carboxylates, and phosphate groups [60]. If the interaction between positively charged TB and negative $-PO_4^-$ groups occurs in a 1 : 1 ratio, TB absorbance would be proportional to the capture probes present on each mm^2 of the spheres' surface (Figure 3(d)); thus the number of capture probes that are immobilized on the total surface of the spheres can be indirectly calculated (Figure 3(d)).

3.4. Topography Analysis of the Spheres before and after miRNA Immobilization. Surface topography of the microspheres was analyzed by AFM to study surface changes (roughness and surface area) before and after miRNA immobilization. AFM analysis (presented in Figures 3(e) and 3(f), before miRNA immobilization, and Figures 3(g), after immobilization) shows a clear alteration in the topography of the surface between pristine surfaces (Figures 3(e) and 3(f), zoomed-in view) and the surfaces after miRNA immobilization (Figure 3(g)). An increased surface roughness (from 6.8 nm to 41.2 nm) was recorded for surfaces of the spheres before and after miRNA immobilization, respectively. As a result of coupling in the hybrid strand, a capture probe shares 12 nucleotides with tagged miRNA analyte. Therefore, the coupled strand contains a total of 33 nucleotides. Knowing the approximate size of each nucleotide (~1 nm), the size of the hybrid strand can be roughly calculated (~33 nm). This number closely corresponds to the improved surface roughness analyzed by AFM (34.4 nm). Additionally, the recorded surface area was found to be ~100-fold greater when comparing surface-immobilized spheres with those before immobilization (from 1 μm^2 to 100.6 μm^2). Such enhancement in the surface area is a direct function of the hybrid strands present on the surface of the bioreceptive microspheres.

3.5. Performance Analysis of the Microspheres in Indirect Detection of miR159. Figure 4(a) shows the calibration curves plotted in a logarithm scale for each microsphere size group conducted in varied concentrations of the labeled miRNA. Increasing correlation coefficient values are observed for MMS-1, MMS-3, and MMS-4, respectively. Figures 4(b) and 4(c) depict fluorescence images of the spheres after detection of 1 nM and 100 nM of the labeled analyte, respectively. According to these images, partial clustering of the spheres has seemingly limited complete analyte-surface interaction. Incorporation of gentle mixing/shaking systems could be a suitable method to allow better accessibility of the spheres to the entire sample volume and to enhance the detection signal further.

Figure 4(d) provides a detection performance comparison among different size groups of the spheres in contrast to their cutoff values (twice the mean values of the negative outcomes, presented in red). The detection signals in this chart are plotted with their original values without subtracting the cutoff values for detailed performance comparison among the size groups. As can be seen, the MMS-1, MMS-2, and MMS-3 groups of the microspheres offered higher detection signal in comparison with the largest size category (MMS-4), when subtracting the cutoff values from the actual detection signals. The overall signal intensity obtained from the developed assay in this study falls within the previously reported values for successful detection of miRNAs using a solid-phase hybridization assay [7, 61]. None of the previously reported detection methods, however, rely on conventional ELISA for the detection miRNAs, which is the point of the current study.

3.6. Performance of the Microspheres in a Competitive Assay. The performance of the spheres was further assessed in a competitive assay. In this protocol, concentration of the fluorescently tagged Cy3-miR159 remained constant, while the concentration of the untagged synthetic miR159 (target analyte) was varied, resulting in decreased fluorescence intensity as the concentration of the target analyte increased. Figure 4(e) represents the result of the competitive assay, which was conducted with the MMS-3 category of the spheres as representative. Concentrations of the untagged miRNA (x-axis) are presented in the logarithm scale, while the y-axis depicts the relative fluorescence intensity. The systematic decrease in fluorescence intensity as a result of increased concentration of the untagged miRNAs provides a clear proof-of-concept that the proposed hybridization assay is an easy and reliable method for quantification of miR159 within this conventional platform.

3.7. Possible Analyte-Surface Interactions. The surface of the microspheres promotes a variety of interaction types between the analyte of interest and the surface. Figure 4(f) schematizes

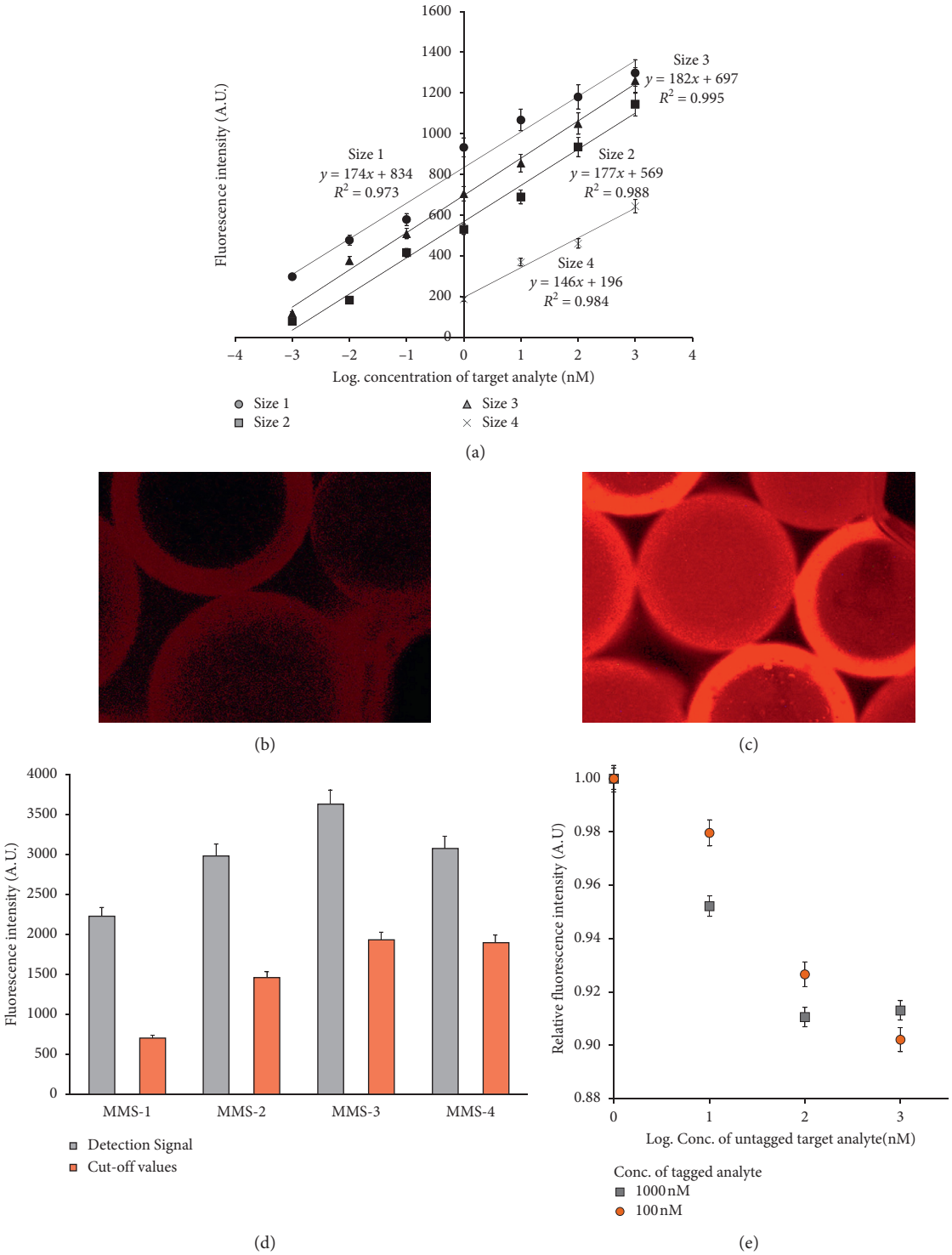

Figure 4: Continued.

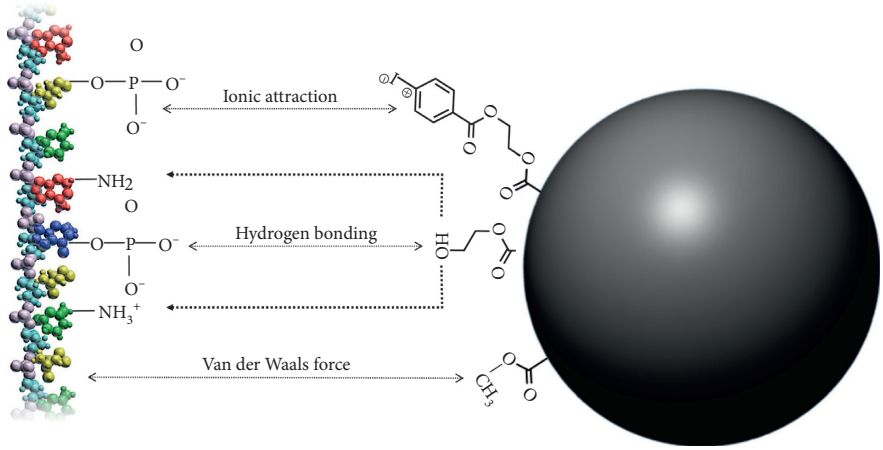

(f)

Figure 4: Performance analysis of the microspheres for detection of miR159: (a) calibration curves plotted for different size categories of the spheres in varied concentrations of the labeled miRNA (1 nM, 10 nM, 100 nM and 1000 nM, 100 pM, 10 pM, and 1 pM); (b, c) fluorescence images of the spheres (MMS-3 as the representative) after detection of 1 nM and 100 nM of the labeled miRNA, respectively; (d) performance analysis of the spheres via indirect detection of miRNA in comparison to the cutoff values, which are twice that of the average negative controls calculated for different size categories (concentration of the labeled miRNA = 1 nM); (e) relative fluorescence signal resulting from competitive assay conducted with a mixture of fluorescent Cy3-miR159 (concentration: 1000 nM or 100 nM) and non-conjugated miR159 at different concentrations (1000, 100, and 10 nM); and (f) schematic representation of the possible physical interactions between the sphere's surface and a capture probe.

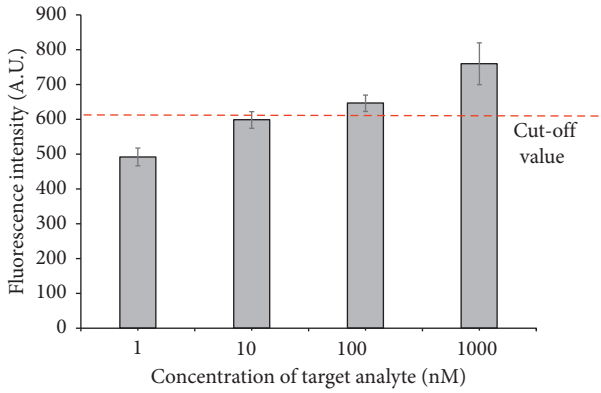

(a)

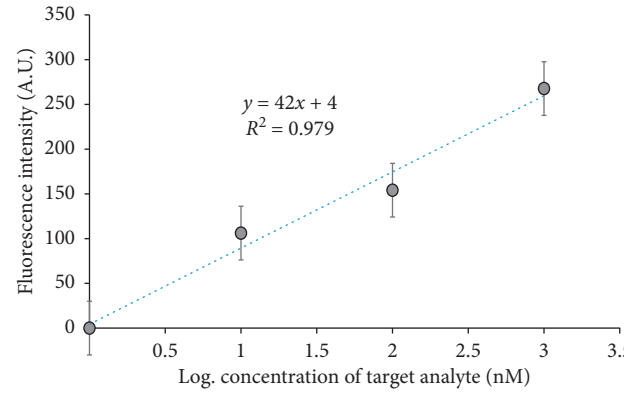

(b)

Detection status	96-wellplate +	96-wellplate −
Positive (TP, FP)	10	8
Negative (FN, TN)	10	2
Total	20	10

Evaluation parameters	96-wellplate
Sensitivity (%)	50
Specificity (%)	80
Accuracy (%)	40
LoD (nM)	15×10^3

(c)

Figure 5: Performance evaluation of conventional 96-well plates: (a) performance analysis of the conventional well plate in miRNA detection (concentration of the labeled miRNA = 1 nM); (b) ELISA calibration curve plotted for varied concentrations of the labeled miRNA (1 nM, 10 nM, 100 nM, and 1000 nM); (c) evaluation of the assay and calculated analytical sensitivity, specificity, accuracy, and LOD.

the possible physical interactions between the engineered surface of the spheres and the nucleotide strands. Hydrogen bonding (H-bond) between the $-PO_4^-$ and the $-NH_2$ groups of the capture probe and -OH groups of the spheres has the highest likelihood. The H-bond occurs between the H atoms of the spheres' -OH groups (O and H are covalently bound) and the N and O atoms of the miRNAs with lone-pair electrons. Furthermore, aromatic rings of the spheres can involve negatively charged $-PO_4^-$ groups of the biomolecules in ionic attraction (electrostatic interaction) [62]. Moreover, carbonyl groups (-C=O) of the spheres could promote van der Waals forces in interaction with the biomolecules [63].

Table 1: Calculated analytical sensitivity, specificity, accuracy, and LOD of the microspheres in miRNA detection.

Detection status	MMS-1		MMS-2		MMS-3		MMS-4	
	+	−	+	−	+	−	+	−
Positive (TP, FP)	20	1	20	3	20	3	20	3
Negative (FN, TN)	0	9	0	8	0	7	0	7
Total	20	10	20	10	20	10	20	10
Sensitivity (%)	100		100		100		100	
Specificity (%)	90		80		70		70	
Accuracy (%)	93		90		86		90	
LOD (pM)	90		40		50		2×10^6	

Table 2: Comparison of the current method with the commercial technologies for miRNA detection.

Platform	Time (min)	Complexity	Accessibility	Specificity	Sensitivity	LOD	References
Gel electrophoresis assays	~280	Moderately complex depending on the assay type	Highly accessible in regular laboratory setups	Standard procedure may induce a chance for nonspecific binding; DNA fragments of interest must be gel-purified and verified to avoid nonspecific bindings	Not suitable for detecting low concentrations	Depends on the assay type (picomolar rage)	[80, 81]
Polymerase chain reaction (PCR)	~35	Complex, expensive, time-consuming, and labor-intensive	Not amenable to many laboratory setups	Highly specific	Accuracy can be compromised by contamination causing amplification of spurious DNA products	Femtomolar range	[65]
Real time polymerase chain reaction (RT-PCR/ qRT-PCR)	~120	Primer design, normalization, and optimization techniques are complex	Involves challenging and individualized processes		High-throughput quantification of miRNAs is error prone		[65, 82]
Polymethacrylate sphere-based assay	~240	Simple and straightforward	Highly accessible in regular laboratory setups	Moderately specific	Highly sensitive	Picomolar range	Current study

Additionally, hydrophobic interaction can play a major role in attracting miRNAs to the surface [62, 64], since the monomers involved in chemical synthesis of the spheres are mostly hydrophobic in their nature [37]. This multitude of physical attraction can strongly influence the biomolecular immobilization and subsequent detection of the miRNAs. Noteworthy that the inherent presence of the surface functional groups on the spheres also promotes covalent attachment of biomolecules to the surface via application of zero-length cross-linking agents or spacer [49, 56].

3.8. Evaluation of the Assay. The assay conducted in a conventional 96-well plate without microspheres was conducted and evaluated for its performance in miRNA detection. Figure 5 provides a detailed analysis of the conventional assay in detection of miR159: (A) detection performance; (B) calibration analysis; and (C) evaluation of the assay. The conventional assay in a 96-well plate shows a rather low detection ability in comparison with the obtained cutoff values that correspond to the negative controls (Figure 5(a)). While the calibration plot refers to a standard linearity level, the assay has proven to suffer from low analytical sensitivity (50%), low accuracy (40%), and unacceptable LOD (Figure 5(c)). A comparison between performance of the 96-well plate with and without microspheres shows a significant detection enhancement due to the presence of microspheres (Figure 5(c)). In particular, size 3 group of the spheres marks a 10-fold higher fluorescence intensity in comparison with that of conventional assay

which enables the detection of challenging biomolecules as miRNAs by *gold standard* technique.

Table 1 summarizes the evaluation parameters for the assay conducted with integrated microspheres. As can be seen, application of the spheres within the conventional assay resulted in 100% analytical sensitivity regardless of the size category. MMS-1, in particular, improved the analytical specificity considerably. Except for MMS-4, all size categories have shown LODs within a picomolar range which is highly desirable for miRNA detection. In the case of MMS-4, recorded standard deviation for lowest concentration of the analyte contributed to the LOD outcome which is not as favorable as those of other size groups. It is noteworthy that the high TB absorption by this size category (MMS-4) does not guarantee its better performance in the analytical assay since the evaluation parameters are also the function of key elements such as the negative control, the calibration curve's slope, and the standard deviation.

While a vast number of reports in the literature provides insight into biodiagnosis strategies, sensitive, selective, accessible, and cost-effective miRNA detection remains a challenge [65]. Circulating miRNAs are present in blood at ng/mL levels. This, according to the length of a fragment, corresponds to a molecular concentration within a picomolar range [66]. Taking the abundance of miRNAs into account, a high level of sensitivity and selectivity is required to detect these challenging bioentities in an effective manner. While several efforts have introduced new methodologies or modified strategies for ultrasensitive targeting miRNAs [67–79], the conventional detection is currently performed by gel electrophoresis assays, polymerase chain reaction (PCR), and real-time polymerase chain reaction (RT-PCR/qRT-PCR). Table 2 provides a comparison between different aspects of commercially applied techniques in comparison with the proposed method here. This table summarizes time, complexity, accessibility, specificity, sensitivity, and LOD for these techniques. While the presented strategy in this study is not as powerful as PCR or qRT-PCR (comparison of the LOD in Table 2), it can be widely accessible in any laboratory setup. This, however, is not the case for PCR/RT-PCR, which is typically operated with highly sophisticated machinery. Further LOD enhancement of the presented strategy can be achieved by incorporating shaking/mixing techniques that would allow spheres to have higher chance of interaction with biomolecules. Comparatively, the proposed strategy offers the least complexity of operation. 96-well plates are available almost in any laboratory setup, and lab technicians familiar with gold standard detection methods could carry out the assay protocols without further training. Most importantly, PCR/RT-PCR is far more inexpensive when compared to the proposed assay while its accuracy might be compromised by contamination.

4. Conclusion

In this work, we have demonstrated a proof-of concept methodology for miRNA detection. Methacrylate microspheres were integrated into a 96-well plate, and immobilized DNA probes were used to capture and detect miR159 within a picomolar range. All important parameters of the assay including analytical sensitivity, specificity, accuracy, and the limit of detection were improved due to the presence of the spheres. This is particularly promising as this simple integration offers the chance of biorecognition for challenging biomolecules including miRNAs within a conventional platform that is typically available in any laboratory setup. Application of the polymer microspheres hold a great potential as they are cost-effective bioreceptive platforms that can be mass-produced in desirable size ranges and with controlled properties depending on the type of desired biorecognition.

Data Availability

All data are presented within the manuscript.

Conflicts of Interest

The authors declare no conflicts of interest.

Authors' Contributions

Samira Hosseini and Patricia Vázquez-Villegas contributed equally to the work. Marc Madou was responsible for conceptualization. Samira Hosseini, Patricia Vázquez-Villegas, and Margarita Sanchez-Dominguez were involved in formal analysis. Sergio Martínez-Chapa carried out funding acquisition. Samira Hosseini, Patricia Vázquez-Villegas, and Leo Koole performed methodology. Marco Rito-Palomares was responsible for project administration. Marco Rito-Palomares and Leo Koole provided resources. Samira Hosseini, Richard Willson, Leo Koole, Marc Madou, and Sergio Martínez-Chapa supervised the study. Samira Hosseini and Marc Madou wrote the original draft. Margarita Sanchez-Dominguez wrote and edited the manuscript.

Acknowledgments

The authors wish to acknowledge the financial support of Tecnológico de Monterrey, Bioprocess and Synthetic Biology Chair (Grant 0821C01004). The authors also would like to acknowledge the financial support of Tecnologico de Monterrey, Mexico, for the special grant (grant number: 002EICII01) awarded to the Nano-sensors and Devices Focus Group, School of Engineering and Sciences, Tecnologico de Monterrey, Monterrey, Mexico. The authors would also like to acknowledge Dr. Oscar E. Vega and Dr. J. Alejandro Arizpe-Zapata (CIMAV S.C. Unidad Monterrey) for conducting AFM analysis and Raman measurements, respectively.

References

[1] K. A. Cissell and S. K. Deo, "Trends in microRNA detection," *Analytical and Bioanalytical Chemistry*, vol. 394, no. 4, pp. 1109–1116, 2009.

[2] N. E. Larkey, L. Zhang, S. S. Lansing, V. Tran, V. L. Seewaldt, and S. M. Burrows, "Förster resonance energy transfer to

impart signal-on and -off capabilities in a single microRNA biosensor," *The Analyst*, vol. 141, no. 22, pp. 6239–6250, 2016.

[3] Y. H. Roh, S. J. Sim, I.-J. Cho, N. Choi, and K. W. Bong, "Vertically encoded tetragonal hydrogel microparticles for multiplexed detection of miRNAs associated with Alzheimer's disease," *The Analyst*, vol. 141, no. 15, pp. 4578–4586, 2016.

[4] Y. Li, J. Zhang, J. Zhao, L. Zhao, Y. Cheng, and Z. Li, "A simple molecular beacon with duplex-specific nuclease amplification for detection of microRNA," *The Analyst*, vol. 141, no. 3, pp. 1071–1076, 2016.

[5] F. Degliangeli, P. P. Pompa, and R. Fiammengo, "Nanotechnology-based strategies for the detection and quantification of MicroRNA," *Chemistry—A European Journal*, vol. 20, no. 31, pp. 9476–9492, 2014.

[6] J. Liu, X. Jiang, R. Zhang et al., "MXene-enabled electrochemical microfluidic biosensor: applications toward multicomponent continuous monitoring in whole blood," *Advanced Functional Materials*, vol. 29, no. 6, Article ID 1807326, 2019.

[7] N. E. Larkey, C. K. Almlie, V. Tran, M. Egan, and S. M. Burrows, "Detection of miRNA using a double-strand displacement biosensor with a self-complementary fluorescent reporter," *Analytical Chemistry*, vol. 86, no. 3, pp. 1853–1863, 2014.

[8] M. de Planell-Saguer and M. C. Rodicio, "Analytical aspects of microRNA in diagnostics: a review," *Analytica Chimica Acta*, vol. 699, no. 2, pp. 134–152, 2011.

[9] Y.-S. Borghei, M. Hosseini, M. R. Ganjali, and S. Hosseinkhani, "Label-free fluorescent detection of microRNA-155 based on synthesis of hairpin DNA-templated copper nanoclusters by etching (top-down approach)," *Sensors and Actuators B: Chemical*, vol. 248, pp. 133–139, 2017.

[10] F. Causa, A. Aliberti, A. M. Cusano, E. Battista, and P. A. Netti, "Supramolecular spectrally encoded microgels with double strand probes for absolute and direct miRNA fluorescence detection at high sensitivity," *Journal of the American Chemical Society*, vol. 137, no. 5, pp. 1758–1761, 2015.

[11] Z. Lu, L. Zhang, Y. Deng, S. Li, and N. He, "Graphene oxide for rapid microRNA detection," *Nanoscale*, vol. 4, no. 19, pp. 5840–5842, 2012.

[12] J.-J. Li, Q. Xi, W.-F. Du, R.-Q. Yu, and J.-H. Jiang, "Label-free fluorescence detection of microRNA based on target induced adenosine2-coralyne-adenosine2 formation," *The Analyst*, vol. 141, no. 8, pp. 2384–2387, 2016.

[13] J. Raez, D. R. Blais, Y. Zhang et al., "Spectroscopically encoded microspheres for antigen biosensing," *Langmuir*, vol. 23, no. 12, pp. 6482–6485, 2007.

[14] R. Bellisario, R. J. Colinas, and K. A. Pass, "Simultaneous measurement of antibodies to three HIV-1 antigens in newborn dried blood-spot specimens using a multiplexed microsphere-based immunoassay," *Early Human Development*, vol. 64, no. 1, pp. 21–25, 2001.

[15] H. Dai, J. Zhu, Z. Yang et al., "A paramagnetic microspheres based automation-friendly rapid chemiluminescent immunoassay method for sensitive detection of chicken interferon-γ," *Chemical Communications*, vol. 49, no. 17, pp. 1708–1710, 2013.

[16] C. C. Hsu, C. E. Wobus, E. K. Steffen, L. K. Riley, and R. S. Livingston, "Development of a microsphere-based serologic multiplexed fluorescent immunoassay and a reverse transcriptase PCR assay to detect murine norovirus 1 infection in mice," *Clinical and Vaccine Immunology*, vol. 12, no. 10, pp. 1145–1151, 2005.

[17] A. J. Johnson, A. J. Noga, O. Kosoy, R. S. Lanciotti, A. A. Johnson, and B. J. Biggerstaff, "Duplex microsphere-based immunoassay for detection of anti-West Nile virus and anti-St. Louis encephalitis virus immunoglobulin M antibodies," *Clinical and Vaccine Immunology*, vol. 12, no. 5, pp. 566–574, 2005.

[18] P. Du and P. Liu, "Novel smart yolk/shell polymer microspheres as a multiply responsive cargo delivery system," *Langmuir*, vol. 30, no. 11, pp. 3060–3068, 2014.

[19] H. Weng, X. Huang, M. Wang, X. Ji, and X. Ge, "Formation of cagelike sulfonated polystyrene microspheres via swelling-osmosis process and loading of CdS nanoparticles," *Langmuir*, vol. 29, no. 49, pp. 15367–15374, 2013.

[20] O. Mero, M.-T. Sougrati, J.-C. Jumas, and S. Margel, "Engineered magnetic core-shell SiO_2/Fe microspheres and "Medusa-like" microspheres of SiO_2/iron oxide/carbon nanofibers or nanotubes," *Langmuir*, vol. 30, no. 32, pp. 9850–9858, 2014.

[21] C. Zhang, J. Luo, L. Ou et al., "Fluorescent porous carbazole-decorated copolymer monodisperse microspheres: facile synthesis, selective and recyclable detection of iron (III) in aqueous medium," *Chemistry—A European Journal*, vol. 24, no. 12, pp. 3030–3037, 2018.

[22] T. A. Taton, C. A. Mirkin, and R. L. Letsinger, "Scanometric DNA array detection with nanoparticle probes," *Science*, vol. 289, no. 5485, pp. 1757–1760, 2000.

[23] A. H. Alhasan, D. Y. Kim, W. L. Daniel et al., "Scanometric microRNA array profiling of prostate cancer markers using spherical nucleic acid-gold nanoparticle conjugates," *Analytical Chemistry*, vol. 84, no. 9, pp. 4153–4160, 2012.

[24] L. Jiang, D. Duan, Y. Shen, and J. Li, "Direct microRNA detection with universal tagged probe and time-resolved fluorescence technology," *Biosensors and Bioelectronics*, vol. 34, no. 1, pp. 291–295, 2012.

[25] L. Wang, Y. Cheng, H. Wang, and Z. Li, "A homogeneous fluorescence sensing platform with water-soluble carbon nanoparticles for detection of microRNA and nuclease activity," *The Analyst*, vol. 137, no. 16, pp. 3667–3672, 2012.

[26] H. Dong, J. Zhang, H. Ju et al., "Highly sensitive multiple microRNA detection based on fluorescence quenching of graphene oxide and isothermal strand-displacement polymerase reaction," *Analytical Chemistry*, vol. 84, no. 10, pp. 4587–4593, 2012.

[27] S. W. Yang and T. Vosch, "Rapid detection of MicroRNA by a silver nanocluster DNA probe," *Analytical Chemistry*, vol. 83, no. 18, pp. 6935–6939, 2011.

[28] B.-Z. Chi, R.-P. Liang, W.-B. Qiu, Y.-H. Yuan, and J.-D. Qiu, "Direct fluorescence detection of microRNA based on enzymatically engineered primer extension poly-thymine (EPEPT) reaction using copper nanoparticles as nano-dye," *Biosensors and Bioelectronics*, vol. 87, pp. 216–221, 2017.

[29] A. E. Prigodich, O.-S. Lee, W. L. Daniel, D. S. Seferos, G. C. Schatz, and C. A. Mirkin, "Tailoring DNA structure to increase target hybridization kinetics on surfaces," *Journal of the American Chemical Society*, vol. 132, no. 31, pp. 10638–10641, 2010.

[30] R. Liu, Q. Wang, Q. Li, X. Yang, K. Wang, and W. Nie, "Surface plasmon resonance biosensor for sensitive detection of microRNA and cancer cell using multiple signal amplification strategy," *Biosensors and Bioelectronics*, vol. 87, pp. 433–438, 2017.

[31] X. Qu, H. Jin, Y. Liu, and Q. Sun, "Strand displacement amplification reaction on quantum dot-encoded silica bead

for visual detection of multiplex MicroRNAs," *Analytical Chemistry*, vol. 90, no. 5, pp. 3482–3489, 2018.

[32] O. A. Goryacheva, A. S. Novikova, D. D. Drozd et al., "Water-dispersed luminescent quantum dots for miRNA detection," *TrAC Trends in Analytical Chemistry*, vol. 111, pp. 197–205, 2019.

[33] S. Hosseini, F. Ibrahim, I. Djordjevic, and L. H. Koole, "Recent advances in surface functionalization techniques on polymethacrylate materials for optical biosensor applications," *The Analyst*, vol. 139, no. 12, pp. 2933–2943, 2014.

[34] S. Hosseini and F. Ibrahim, *Current Optical Biosensors in Clinical Practice: Novel Polymeric Biochips for Enhanced Detection of Infectious Diseases*, Springer, Berlin, Germany, 2016.

[35] A. R. Chin, M. Y. Fong, G. Somlo et al., "Cross-kingdom inhibition of breast cancer growth by plant miR159," *Cell Research*, vol. 26, no. 2, pp. 217–228, 2016.

[36] S. Hosseini, M. M. Aeinehvand, S. M. Uddin et al., "Microsphere integrated microfluidic disk: synergy of two techniques for rapid and ultrasensitive dengue detection," *Scientific Reports*, vol. 5, no. 1, 2015.

[37] K. Saralidze, C. van Hooy-Corstjens, L. Koole, and M. Knetsch, "New acrylic microspheres for arterial embolization: combining radiopacity for precise localization with immobilized thrombin to trigger local blood coagulation," *Biomaterials*, vol. 28, no. 15, pp. 2457–2464, 2007.

[38] S. Sano, K. Kato, and Y. Ikada, "Introduction of functional groups onto the surface of polyethylene for protein immobilization," *Biomaterials*, vol. 14, no. 11, pp. 817–822, 1993.

[39] I. Djordjevic, N. R. Choudhury, N. K. Dutta, S. Kumar, E. J. Szili, and D. A. Steele, "Polyoctanediol citrate/sebacate bioelastomer films: surface morphology, chemistry and functionality," *Journal of Biomaterials Science, Polymer Edition*, vol. 21, no. 2, pp. 237–251, 2010.

[40] S. Hosseini, F. Ibrahim, I. Djordjevic, and L. H. Koole, "Polymethyl methacrylate-co-methacrylic acid coatings with controllable concentration of surface carboxyl groups: a novel approach in fabrication of polymeric platforms for potential bio-diagnostic devices," *Applied Surface Science*, vol. 300, pp. 43–50, 2014.

[41] S. Alcon, A. Talarmin, M. Debruyne, A. Falconar, V. Deubel, and M. Flamand, "Enzyme-linked immunosorbent assay specific to dengue virus type 1 nonstructural protein NS1 reveals circulation of the antigen in the blood during the acute phase of disease in patients experiencing primary or secondary infections," *Journal of Clinical Microbiology*, vol. 40, no. 2, pp. 376–381, 2002.

[42] E. M. Linares, C. S. Pannuti, L. T. Kubota, and S. Thalhammer, "Immunospot assay based on fluorescent nanoparticles for dengue fever detection," *Biosensors and Bioelectronics*, vol. 41, pp. 180–185, 2013.

[43] S. J. Reinholt, A. Sonnenfeldt, A. Naik, M. W. Frey, and A. J. Baeumner, "Developing new materials for paper-based diagnostics using electrospun nanofibers," *Analytical and Bioanalytical Chemistry*, vol. 406, no. 14, pp. 3297–3304, 2014.

[44] A. Shrivastava and V. Gupta, "Methods for the determination of limit of detection and limit of quantitation of the analytical methods," *Chronicles of Young Scientists*, vol. 2, no. 1, p. 21, 2011.

[45] N. Swamy, K. N. Prashanth, and K. Basavaiah, "Titrimetric and spectrophotometric assay of diethylcarbamazine citrate in formulations using iodate and iodide mixture as reagents," *Brazilian Journal of Pharmaceutical Sciences*, vol. 51, no. 1, pp. 43–52, 2015.

[46] M. Gad, H. Zaazaa, S. Amer, and M. Korany, "Static headspace gas chromatographic method for the determination of residual solvents in cephalosporins," *RSC Advances*, vol. 5, no. 22, pp. 17150–17159, 2015.

[47] S. M. Bauer, M. Gehringer, and S. A. Laufer, "A direct enzyme-linked immunosorbent assay (ELISA) for the quantitative evaluation of Janus Kinase 3 (JAK3) inhibitors," *Analytical Methods*, vol. 6, no. 21, pp. 8817–8822, 2014.

[48] A. G. Pereira, F. B. D'Avila, P. C. L. Ferreira, M. G. Holler, R. P. Limberger, and P. E. Fröehlich, "Determination of cocaine, its metabolites and pyrolytic products by LC-MS using a chemometric approach," *Analytical Methods*, vol. 6, no. 2, pp. 456–462, 2014.

[49] J. M. Goddard and J. H. Hotchkiss, "Polymer surface modification for the attachment of bioactive compounds," *Progress in Polymer Science*, vol. 32, no. 7, pp. 698–725, 2007.

[50] J. L. Koenig, *Spectroscopy of Polymers*, Elsevier, Amsterdam, Netherlands, 1999.

[51] T. H. Qazi, R. Rai, and A. R. Boccaccini, "Tissue engineering of electrically responsive tissues using polyaniline based polymers: a review," *Biomaterials*, vol. 35, no. 33, pp. 9068–9086, 2014.

[52] E. Evlyukhin, L. Museur, M. Traore, C. Perruchot, A. Zerr, and A. Kanaev, "A new route for high-purity organic materials: high-pressure-ramp-induced ultrafast polymerization of 2-(hydroxyethyl) methacrylate," *Scientific Reports*, vol. 5, p. 18244, 2015.

[53] C. C. Bonang and S. M. Cameron, "Resonance Raman and hyper-Raman scattering from monosubstituted benzenes," *Chemical Physics Letters*, vol. 187, no. 6, pp. 619–622, 1991.

[54] C. Navarra, M. Cadenaro, A. Frassetto, L. Fontanive, R. Di Lenarda, and L. Breschi, "Degree of conversion of self-etch adhesives: in situ micro-Raman analysis," *Operative Dentistry*, vol. 41, no. 5, pp. 501–510, 2016.

[55] K. Thomas, M. Sheeba, V. Nampoori, C. Vallabhan, and P. Radhakrishnan, "Raman spectra of polymethyl methacrylate optical fibres excited by a 532 nm diode pumped solid state laser," *Journal of Optics A: Pure and Applied Optics*, vol. 10, Article ID 055303, 2008.

[56] Y. Bai, C. G. Koh, M. Boreman et al., "Surface modification for enhancing antibody binding on polymer-based microfluidic device for enzyme-linked immunosorbent assay," *Langmuir*, vol. 22, no. 22, pp. 9458–9467, 2006.

[57] S. Hosseini, F. Ibrahim, I. Djordjevic et al., "Synthesis and processing of ELISA polymer substitute: the influence of surface chemistry and morphology on detection sensitivity," *Applied Surface Science*, vol. 317, pp. 630–638, 2014.

[58] J. Jebaramya, M. Ilanchelian, and S. Prabahar, "Spectral studies of toluidine blue o in the presence of sodium dodecyl sulfate," *Sensors*, vol. 21, p. 22, 2009.

[59] H. G. Hansma, I. Revenko, K. Kim, and D. E. Laney, "Atomic force microscopy of long and short double-stranded, single-stranded and triple-stranded nucleic acids," *Nucleic Acids Research*, vol. 24, no. 4, pp. 713–720, 1996.

[60] G. Sridharan and A. Shankar, "Toluidine blue: a review of its chemistry and clinical utility," *Journal of Oral and Maxillofacial Pathology*, vol. 16, no. 2, pp. 251–255, 2012.

[61] H. Arata, H. Komatsu, A. Han, K. Hosokawa, and M. Maeda, "Rapid microRNA detection using power-free microfluidic chip: coaxial stacking effect enhances the sandwich hybridization," *The Analyst*, vol. 137, no. 14, pp. 3234–3237, 2012.

[62] J.-Y. Yoon, H.-Y. Park, J.-H. Kim, and W.-S. Kim, "Adsorption of BSA on highly carboxylated microspheres-quantitative effects of surface functional groups and

interaction forces," *Journal of Colloid and Interface Science*, vol. 177, no. 2, pp. 613–620, 1996.

[63] S. H. Lee and E. Ruckenstein, "Adsorption of proteins onto polymeric surfaces of different hydrophilicities-a case study with bovine serum albumin," *Journal of Colloid and Interface Science*, vol. 125, no. 2, pp. 365–379, 1988.

[64] A. Kondo and K. Higashitani, "Adsorption of model proteins with wide variation in molecular properties on colloidal particles," *Journal of Colloid and Interface Science*, vol. 150, no. 2, pp. 344–351, 1992.

[65] T. Tian, J. Wang, and X. Zhou, "A review: microRNA detection methods," *Organic & Biomolecular Chemistry*, vol. 13, no. 8, pp. 2226–2238, 2015.

[66] S. O. Kelley, "What are clinically relevant levels of cellular and biomolecular analytes?" *ACS Sensors*, vol. 2, no. 2, pp. 193–197, 2017.

[67] M. N. Islam, M. K. Masud, N.-T. Nguyen et al., "Gold-loaded nanoporous ferric oxide nanocubes for electrocatalytic detection of microRNA at attomolar level," *Biosensors and Bioelectronics*, vol. 101, pp. 275–281, 2018.

[68] H. Yang, A. Hui, G. Pampalakis et al., "Direct, electronic microRNA detection for the rapid determination of differential expression profiles," *Angewandte Chemie International Edition*, vol. 48, no. 45, pp. 8461–8464, 2009.

[69] M. N. Islam, S. Moriam, M. Umer et al., "Naked-eye and electrochemical detection of isothermally amplified HOTAIR long non-coding RNA," *The Analyst*, vol. 143, no. 13, pp. 3021–3028, 2018.

[70] M. K. Masud, M. N. Islam, M. H. Haque et al., "Gold-loaded nanoporous superparamagnetic nanocubes for catalytic signal amplification in detecting miRNA," *Chemical Communications*, vol. 53, pp. 8231–8234, 2017.

[71] K. M. Koo, L. G. Carrascosa, M. J. A. Shiddiky, and M. Trau, "Amplification-free detection of gene fusions in prostate cancer urinary samples using mRNA-gold affinity interactions," *Analytical Chemistry*, vol. 88, no. 13, pp. 6781–6788, 2016.

[72] K. M. Koo, L. G. Carrascosa, M. J. A. Shiddiky, and M. Trau, "Polyextensions of miRNAs for amplification-free electrochemical detection on screen-printed gold electrodes," *Analytical Chemistry*, vol. 88, no. 4, pp. 2000–2005, 2016.

[73] H. Lee, J.-E. Park, and J.-M. Nam, "Bio-barcode gel assay for microRNA," *Nature Communications*, vol. 5, no. 1, p. 3367, 2014.

[74] C. Wang, Q. Ding, P. Plant et al., "Droplet digital PCR improves urinary exosomal miRNA detection compared to real-time PCR," *Clinical Biochemistry*, vol. 67, pp. 54–59, 2019.

[75] B. Tian, Z. Qiu, J. Ma et al., "On-particle rolling circle amplification-based core-satellite magnetic superstructures for microRNA detection," *ACS Applied Materials & Interfaces*, vol. 10, no. 3, pp. 2957–2964, 2018.

[76] R. Tian, Y. Li, and J. Bai, "Hierarchical assembled nanomaterial paper based analytical devices for simultaneously electrochemical detection of microRNAs," *Analytica Chimica Acta*, vol. 1058, pp. 89–96, 2019.

[77] Z.-Z. Yang, Z.-B. Wen, X. Peng, Y.-Q. Chai, W.-B. Liang, and R. Yuan, "A novel fluorescent assay for the ultrasensitive detection of miRNA-21 with the use of G-quadruplex structures as an immobilization material for a signal indicator," *Chemical Communications*, vol. 55, no. 45, pp. 6453–6456, 2019.

[78] J. Wang, J. Lu, S. Dong et al., "An ultrasensitive electrochemical biosensor for detection of microRNA-21 based on redox reaction of ascorbic acid/iodine and duplex-specific nuclease assisted target recycling," *Biosensors and Bioelectronics*, vol. 130, pp. 81–87, 2019.

[79] T. Xue, W. Liang, Y. Li et al., "Ultrasensitive detection of miRNA with an antimonene-based surface plasmon resonance sensor," *Nature Communications*, vol. 10, p. 28, 2019.

[80] https://www.thermofisher.com/mx/es/home/life-science/pcr/real-time-pcr/real-time-pcr-learning-center/real-time-pcr-basics/benefits-fast-real-time-pcr.html.

[81] A. Drabik, A. Bodzoń-Kułakowska, and J. Silberring, "Gel electrophoresis," in *Proteomic Profiling and Analytical Chemistry*, P. Ciborowski and J. Silberring, Eds., pp. 115–143, Elsevier, Boston, MA, USA, 2nd edition, 2016.

[82] E. Varkonyi-Gasic, R. Wu, M. Wood, E. F. Walton, and R. P. Hellens, "Protocol: a highly sensitive RT-PCR method for detection and quantification of microRNAs," *Plant Methods*, vol. 3, no. 1, p. 12, 2007.